Title

A therapeutic small molecule enhances γ-oscillations and improves cognition/memory in Alzheimers disease model mice.

Journal

Proceedings of the National Academy of Sciences, 121(33)

Authors

Wei, Xiaofei
Campagna, Jesus
Jagodzinska, Barbara
et al.

Publication Date

2024-08-13

DOI

10.1073/pnas.2400420121

Peer reviewed

PNAS RESEARCH ARTICLE | PHARMACOLOGY OPEN ACCESS

A therapeutic small molecule enhances γ-oscillations and improves cognition/memory in Alzheimer's disease model mice

Xiaofei Wei[a,b,1], Jesus J. Campagna[c,1], Barbara Jagodzinska[c], Dongwook Wi[c], Whitaker Cohn[c], Jessica T. Lee[c], Chunni Zhu[c], Christine S. Huang[d], László Molnár[e], Carolyn R. Houser[d], Varghese John[c], and Istvan Mody[a,f,2]

Affiliations are included on p. 10.

Edited by Vikaas S. Sohal, University of California—San Francisco, CA; received January 8, 2024; accepted July 8, 2024 by Editorial Board Member Susan G. Amara

Brain rhythms provide the timing for recruitment of brain activity required for linking together neuronal ensembles engaged in specific tasks. The γ-oscillations (30 to 120 Hz) orchestrate neuronal circuits underlying cognitive processes and working memory. These oscillations are reduced in numerous neurological and psychiatric disorders, including early cognitive decline in Alzheimer's disease (AD). Here, we report on a potent brain-permeable small molecule, DDL-920 that increases γ-oscillations and improves cognition/memory in a mouse model of AD, thus showing promise as a class of therapeutics for AD. We employed anatomical, in vitro and in vivo electrophysiological, and behavioral methods to examine the effects of our lead therapeutic candidate small molecule. As a novel in central nervous system pharmacotherapy, our lead molecule acts as a potent, efficacious, and selective negative allosteric modulator of the γ-aminobutyric acid type A receptors most likely assembled from α1β2δ subunits. These receptors, identified through anatomical and pharmacological means, underlie the tonic inhibition of parvalbumin (PV) expressing interneurons (PV+INs) critically involved in the generation of γ-oscillations. When orally administered twice daily for 2 wk, DDL-920 restored the cognitive/memory impairments of 3- to 4-mo-old AD model mice as measured by their performance in the Barnes maze. Our approach is unique as it is meant to enhance cognitive performance and working memory in a state-dependent manner by engaging and amplifying the brain's endogenous γ-oscillations through enhancing the function of PV+INs.

gamma oscillations | parvalbumin | interneurons | GABA-A receptors | Alzheimer's disease

Significance

Wei et al., have studied the subunit composition of γ-aminobutyric acid type A receptors responsible for the tonic inhibition of parvalbumin positive interneurons and identified a small molecule (DDL-920) as a potent, efficacious, and selective negative allosteric modulator of these receptors. DDL-920 increases the power of γ-oscillations following oral administration and remedies the memory impairment of Alzheimer's disease model mice in the Barnes maze.

The fundamental pathology of Alzheimer's disease (AD) is largely understood (1), yet there are no effective drugs to restore cognition and memory in AD patients. Aducanumab (Aduhelm®) and lecanemab (Leqembi®) were recently approved by the FDA for treatment of AD, however, the approvals were based on significant decreases in the brain amyloid-β (Aβ) pathology, while their ability to reverse cognitive impairment was modest, and side effects still remain a concern (2). Cognitive impairment in AD refers to the states of confusion or memory loss that increase yearly in frequency and/or progress in severity. Mild cognitive impairment (MCI) is a condition with more memory problems than what is considered normal for a given age, with symptoms less severe than in AD. About 80% of individuals who fit the definition of amnestic MCI go on to develop AD within 7 y. In a large cohort, prediagnostic cognitive impairment and decline with time were present in patients diagnosed 9 y later with AD (3). Although age is the primary risk factor for cognitive impairment, other common neurological and psychiatric conditions such as epilepsy (4), Parkinson's disease (5), traumatic brain injury (6), autism spectrum disorder (7), depression (8), schizophrenia (9), and numerous other morbidities are plagued by loss of cognitive performance. A vast literature has demonstrated that the γ-oscillations generated by fast-spiking, parvalbumin-containing interneurons (PV+INs) constitute a fundamental binding scheme and timing mechanism for bringing together brain networks critical for cognitive performance and short-term or working memory (10–20). Considerable evidence exists that the neurological and psychiatric disorders mentioned above are also characterized by reduced γ-oscillations (20, 21).

High temporal resolution recording methods, such as magnetoencephalography (MEG) (22), have made it clear that AD patients starting as early as at the MCI stage have diminished γ-oscillations even before the Aβ load takes full effect (23, 24). Moreover, it has been well established that almost all AD mouse models have diminished γ-oscillations. (23) Restoring γ-oscillations in AD patients has yet to be attempted, but remarkably, optogenetic stimulation of PV+INs at a typical γ-oscillation frequency (40 Hz) reduced

Author contributions: J.J.C., C.R.H., V.J., and I.M. designed research; X.W., J.J.C., B.J., D.W., W.C., J.T.L., C.Z., C.S.H., C.R.H., V.J., and I.M. performed research; L.M. and I.M. contributed new reagents/analytic tools; X.W., J.J.C., B.J., C.S.H., L.M., C.R.H., V.J., and I.M. analyzed data; and C.R.H., V.J., and I.M. wrote the paper.

Competing interest statement: Composition and methods for treating neurodgenerative diseases. W.I.P. Organization, ed. (The Regents of the University of California).

This article is a PNAS Direct Submission. V.S.S. is a guest editor invited by the Editorial Board.

[1]X.W. and J.J.C. contributed equally to this work.

[2]To whom correspondence may be addressed. Email: mody@ucla.edu.

This article contains supporting information online at https://www.pnas.org/lookup/suppl/doi:10.1073/pnas.2400420121/-/DCSupplemental.

Published August 6, 2024.

plaque burden in a mouse model of AD (25), and sensory (visual and auditory) stimuli (26, 27) delivered on a daily basis were also effective. These latter methods may well be easily applicable to humans (28) for cognitive enhancement therapies. Accordingly, scores of clinical trials are underway (29) using transcranial magnetic stimulation (TMS), transcranial alternating or direct current stimulation (tACS or tDCS), GammaSense stimulation, transcranial electromagnetic treatment, and intranasal delivery of near-infrared light via diodes, all aimed at reducing hyperexcitability and/or improving cognition in AD. However, the timing of the external stimuli will rarely, if ever, coincide with the demand for endogenous γ-oscillations in the brain (30–32). A recent study (32) failed to replicate the plaque-clearing effects of 40 Hz stimulation (25) and pointed out the inability of external periodic stimuli to engage γ-oscillations in the brain. We therefore decided to pursue a pharmacological approach to enhance the endogenous γ-oscillations of the brain by reducing the tonic inhibition of PV+INs. This approach should work when these natural rhythms are engaged by the brain's own circuitry during cognitive demand and working memory (33–36).

Results

The Specific $GABA_AR$ Partnership Responsible for the Tonic Inhibition of PV+INs. In the Cys-loop superfamily of ligand-gated ion channels, the $GABA_ARs$ stand out as the most diverse based on subunit composition and pharmacology. From nearly 500,000 possible heteropentameric combinations of 19 different subunits, due to specific receptor partnership rules, there are only about 26 naturally occurring subtypes in the brain (37), but these may be augmented by the recently discovered diversity of receptor assembly (38). As various subunits impart specific biophysical properties such as channel open times, desensitization, deactivation, GABA affinity, and potency, they also define a wide array of pharmacological properties that modulate the function of these receptors (37). The following native $GABA_ARs$ with δ-subunits are present in the brain (39): α6β2δ are abundant on cerebellar granule cells; α4β2/3δ are most prominent in the forebrain in dentate gyrus granule cells, various thalamic neurons, medium spiny striatal neurons, neocortical pyramidal cells, and other cell types. The δ-subunits assemble with α1-subunits only in a small specific subset of neurons, the PV+INs (40–44), and possibly the neurogliaform cells (41, 43, 45), which actually decouple pyramidal cells from γ-oscillations (46). It is intriguing that in the brain's native $GABA_ARs$, the δ-subunits seem to partner with only three (α1, α4, and α6) of the six different α subunits. Moreover, the factors governing α/δ-subunit assembly are most likely cell-specific, as when α4 or α6 subunits are genetically deleted from mice, the δ- subunits fail to pair up with existing α1 subunits. Accordingly, cells with deleted α4 or α6 subunits also become δ subunit knockouts (43, 47).

Using conventional microscopy, we have previously shown the colocalization of δ-subunits in PV+INs of the CA3 region (42). We have now extended these findings using confocal microscopy to the localization of α1 subunits in the PV+INs of this region (Fig. 1*A*). We also confirmed the colocalization of

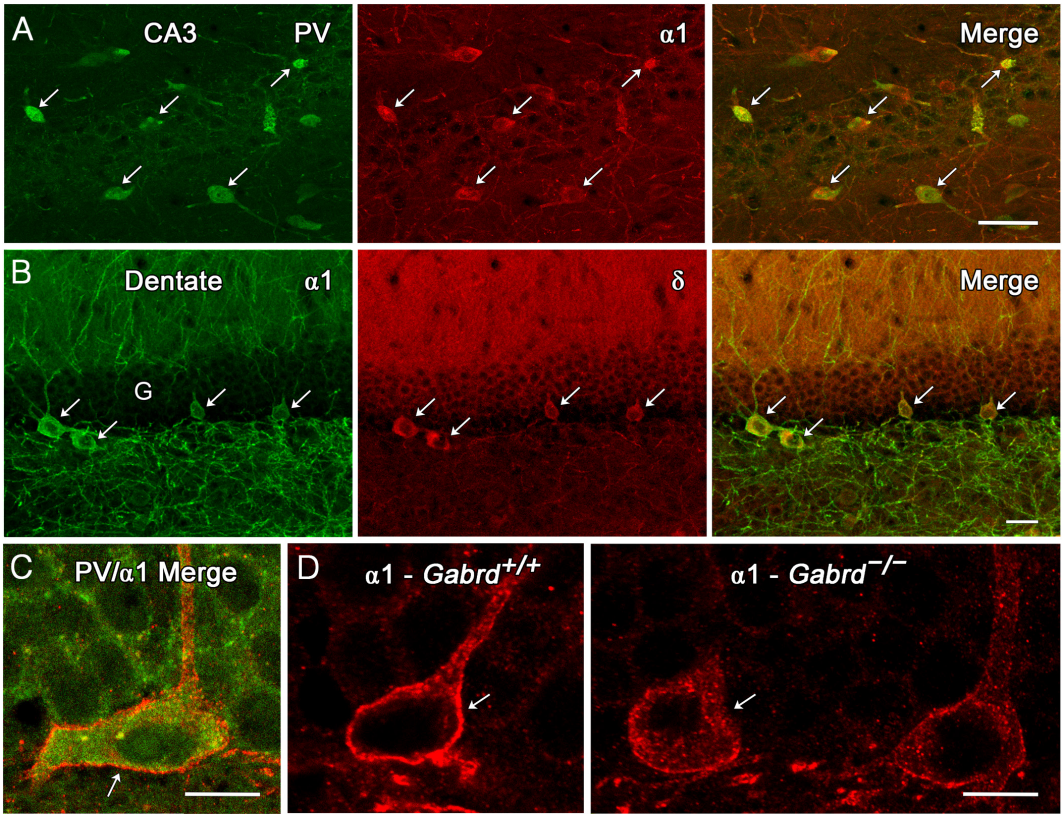

Fig. 1. α1 subunit is prominently expressed in PV+ interneurons in CA3 and in similar interneurons along the base of the dentate granule cell layer. (*A*) Many PV+INs in CA3 express the α1 subunit (examples at arrows). Their distribution closely resembles that of δ subunit-expressing PV+INs in CA3 [described previously (42)]. (*B*) In the dentate gyrus, the α1 subunit is strongly expressed on δ subunit-containing interneurons (arrows) along the base of the granule cell layer (G). (*C*) PV+INs in this location also exhibit strong α1 subunit labeling along their cell surface (arrow). (*D*) In $Gabrd^{+/+}$ animals, α1 subunit labeling is similarly expressed on the surface of these interneurons, with lighter, diffuse labeling within the cytoplasm. In contrast, in $Gabrd^{-/-}$ animals, many α1-labeled interneurons have reduced surface labeling (arrow) and exhibit increased punctate labeling within the cytoplasm. This suggests that loss of the δ subunit leads to altered localization of the α1 subunit in these interneurons, consistent with a favored partnership of the δ and α1 subunits. (Scale bars: *A* = 50 μm; *B* = 20 μm; *C* and *D* = 10 μm.)

α1 and δ subunits in the characteristically pyramidal-shaped PV+INs (basket cells) of the dentate gyrus (Fig. 1 *B* and *C* and *SI Appendix*, Figs. S1 *A–F* and S2*A*). We next set out to examine the strength of α1/δ-subunit partnership in the same neurons when δ-subunits were absent following genetic deletion. We observed strong membrane staining of α1 subunits in PV+INs of WT ($Gabrd^{+/+}$) mice over the entire extent of the cells (Fig. 1*D*), consistent with an extrasynaptic localization of these receptors. In sharp contrast, α1-subunit surface labeling was decreased with α1-subunits trapped in the cytoplasm in homozygous δ-subunit knock-out ($Gabrd^{-/-}$) mice (Fig. 1*D*), indicating that the α1/δ-subunit partnership is critical for ensuring surface expression of these subunit combinations (*SI Appendix*, Fig. S2*A*). We have also identified the predominant type of β subunit present in the PV+IN $GABA_AR$ assembly as the β2 variant (*SI Appendix*, Fig. S2*B*), while finding only limited staining for β3 subunits (*SI Appendix*, Fig. S2*C*). These data strongly corroborate the α1β2δ subunit composition of the extrasynaptic $GABA_ARs$ of PV+INs, likely to be responsible for their tonic GABA conductance, consistent with a previous anatomical report (44). We did not stain for β1 subunits, as a recent large-scale proteomic study in PV+INs (48) has excluded their presence. The same study also showed a fourfold larger abundance of β2 subunit protein compared to β3, confirming our anatomical results. However, at this time we cannot ascertain the precise stoichiometry of the extrasynaptic α1β2δ $GABA_ARs$ of PV+INs, since they may show quite unusual assembly rules as recently shown for α4β3δ $GABA_ARs$ (38).

Pharmacological Specificity and Selectivity of the α1β2δ $GABA_ARs$ Underlying Tonic Inhibition of PV+INs. There are notable differences between the properties of $GABA_ARs$ with δ-subunits (δ-$GABA_ARs$) depending on the α subunit present. In expression systems (*Xenopus* oocytes, HEK cells), the potency of GABA is higher at α4 versus α1 containing δ-$GABA_ARs$. The EC50 of GABA at α4δ-$GABA_ARs$ is in the high nM range (49–51), while at α1δ-$GABA_ARs$ it is about 10-fold higher (low μM) (49–54). This raises an interesting question about when exactly the α1δ-$GABA_ARs$ of PV+INs (40–44) and those on cortical and hippocampal neurogliaform cells (41, 43, 45) become activated? The high activity of PV+INs during γ-oscillations (10, 1117, 55), must generate sufficient (low μM) GABA for the α1δ-$GABA_ARs$ of PV+INs to become activated, thus controlling γ-oscillation frequency and amplitude. However, during γ-oscillations, the same receptors on neurogliaform cells will not be active, as these cells do not partake in γ-oscillations (46, 56, 57). There are also differences in the effects of positive allosteric modulators (PAM) on δ-$GABA_ARs$ that depend on the presence of different α subunits. Whereas the effects of neurosteroids such as allopregnanolone and THDOC appear to be similar irrespective of the α subunits, the effects of ethanol and the δ-$GABA_AR$ selective modulator DS2 show different activities in expression systems compared to the native receptors in the brain. In expression systems DS2 is equally potent at α4- and α1δ-$GABA_ARs$ (50, 52, 58, 59), yet DS2, in sharp contrast to allopregnanolone, does not alter γ-oscillations in slices with native α1δ-$GABA_ARs$ (40, 42). It is interesting to note that in oocytes, tracazolate, a nonbenzodiazepine anxiolytic, selectively increases both the potency and efficacy of GABA in receptors with α1β2δ composition (53). As the same subunits appear to constitute the extrasynaptic $GABA_ARs$ of PV+INs, we decided to test the effects of tracazolate on the tonic and phasic inhibition of PV+INs to ascertain also by pharmacological means whether $GABA_ARs$ with α1β2δ composition were present. As shown in Fig. 2*A*, tracazolate at 10 μM, the effective concentration in oocytes (53), significantly enhanced the tonic currents recorded in the absence of added GABA (control: 0.86 ± 0.45 A/F vs 10 μM tracazolate: 1.56 ± 0.36 A/F, mean ± SD, n = 5 cells, n = 5 mice; an 82% increase, $P = 0.0139$, paired *t*-test) of PV+INs, supporting the involvement of α1β2δ $GABA_ARs$ in mediating the tonic GABA conductance.

We next wanted to test the effects of our potential negative allosteric modulator (NAM) compound DDL-920 on the same neurons. The SMILES and chemical structures of DDL-920 are shown in *SI Appendix*, Table S1, and its synthesis is published in our international patent application (60). We made patch-clamp recordings from PV+INs identified by IR-DIC and fluorescence in an immersion-type rapid flow-through chamber. At concentrations as low as 1 nM, DDL-920 reduced the large tonic currents elicited by 5 μM GABA in PV+INs (Fig. 2*B*; control: 4.78 ± 3.75 A/F vs. 1 nM DDL-920: 1.39 ± 1.16 A/F, mean ± SD, n = 6 cells, n = 6 mice; a 71% decrease, $P = 0.0253$, paired *t*-test). As tonic inhibition in PV+INs is mediated by extrasynaptic α1β2δ $GABA_AR$ (see previous section), while phasic inhibition is generated by fast synaptic α1β2γ2 receptors (61), a differential effect of DDL-920 on the tonic vs. phasic currents will indicate how specific this compound is for the native α1β2δ $GABA_ARs$ of PV+INs. In a different set of experiments, we measured the compound's tonic vs phasic specificity by plotting the fraction blocked of the tonic current vs that of the phasic current (Fig. 2*C*). The fractions blocked are calculated as 1 – (current in drug/current in control). The specificity for the inhibition of the tonic vs. phasic current was calculated as fraction blocked (tonic/phasic). For 1 nM DDL-920, this value is 0.792/0.011, i.e., 72-fold. We further examined the selectivity of DDL-920 for the α1β2δ $GABA_ARs$ found in PV+INs by comparing its effects on δ-$GABA_ARs$ with a different α-subunit, the α4β2δ $GABA_ARs$ responsible for tonic inhibition in dentate gyrus granule cells (62). DDL-920 at 1 nM was approximately twofold more selective for the tonic currents mediated by α1β2δ $GABA_ARs$ in PV+INs than those of dentate gyrus granule cells mediated by α4β2δ $GABA_ARs$ (Fig. 2*C*). Naturally, a full comparison with other δ-$GABA_ARs$ with different α-subunits in various cell types will have to follow. We did not perform a full dose–response analysis of the effects of DDL-920 on the tonic GABA currents of PV+INs, as we aimed to stay within the range of concentrations we found in the brains of mice after subcutaneous (SQ) or oral administration at a standard dose of 10 mg/kg (*SI Appendix*, Fig. S3 *A* and *B*). However, from the three doses of DDL-920 examined on the tonic inhibition of PV+INs in vitro (Fig. 2*C*), it appears that the compound already reaches full efficacy at 1 nM.

We next engaged in some molecular modeling of DDL-920 binding to the available $GABA_AR$ homo- and heteropentameric structures resolved through protein crystallography or cryo-EM. The docking of the DDL-920 molecule to the homomeric human β3 $GABA_AR$ (pdb: 4COF) is shown in *SI Appendix*, Fig. S4*A*. The binding gives a good lead finder (LF) rank score of -10.34 which is further improved with the addition of the $GABA_AR$ δ -subunit (pdb: 7QND; *SI Appendix*, Fig. S4*B*). Unfortunately, the precise structural model for the unique α1β2δ $GABA_AR$ combination found on PV+INs is not available, but our modeling shows that the introduction of the δ subunit provides additional binding sites for DDL-920. Using the β3 $GABA_AR$ subunit in our model instead of the β2 is not a great concern, as in the regions where DDL-920 appears to bind, there is nearly a 100% homology between the two subunits. Notably, the Phe200 residue on the β2 (fully conserved in β3, both mouse and human) that is critical for the GABA binding site at the α1–β2 interface (63) is also a key residue for the DDL-920 binding (*SI Appendix*, Fig. S4*A*) suggesting

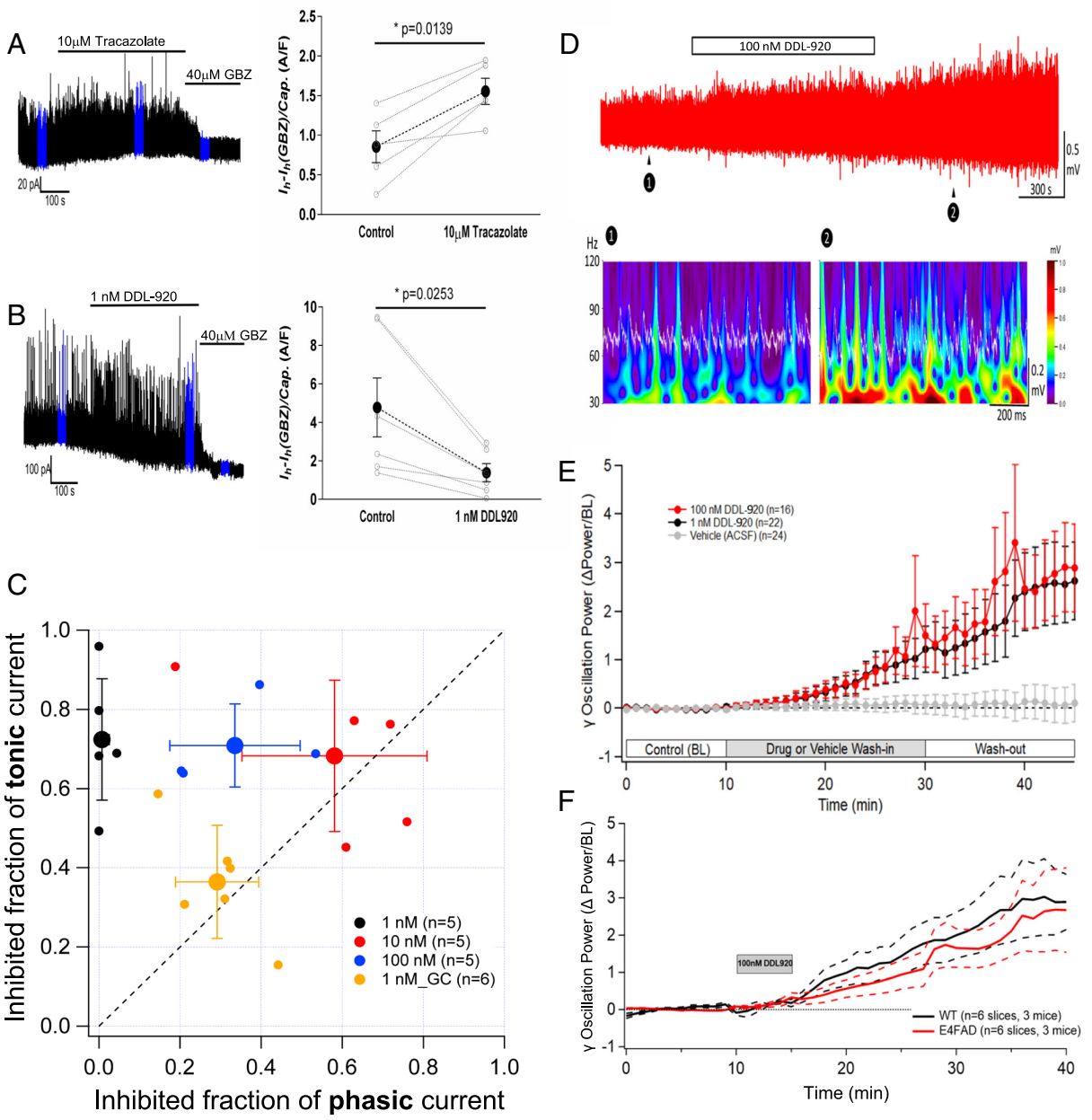

Fig. 2. Pharmacological characterization of DDL-920 in PV+INs and its effects on γ-oscillations in vitro. (*A*) The effects of tracazolate, a compound known to potentiate $GABA_A$Rs composed of α1β2δ subunits in *Xenopus* oocytes, on the tonic $GABA_A$R-mediated currents of identified PV+INs. Left panel: Raw traces of a voltage-clamp recording at Vh = 0 mV of the tonic $GABA_A$R-mediated currents before, during, and after the perfusion of 10 μM tracazolate (horizontal bar). The perfusion of 40 μM gabazine (GBZ) was used to block all $GABA_A$Rs. The *blue* segments in the recording indicate the 30 s epochs used for the tonic and phasic current analysis. *Right panel*: Summary data from 5 recordings where the tonic $GABA_A$R-mediated currents normalized to the capacitance of the cells are plotted before (Control) and during (10 μM tracazolate) the perfusion of the drug. The individual experimental results are illustrated with light gray open circles connected by dotted lines, while the averages (± SEM) are indicated by solid black circles connected by a black dotted line. The p-value indicates a significant increase in the tonic current as determined using the paired Wilcoxon signed-rank test. (*B*) The effects of DDL-920 on the tonic $GABA_A$R-mediated currents of identified PV+INs. Left panel: Raw traces of a voltage-clamp recording at Vh=0 mV of the tonic $GABA_A$R-mediated currents before, during, and after the perfusion of 1 nM DDL-920 (horizontal bar). The perfusion of 40 μM gabazine (GBZ) was used to block all $GABA_A$Rs. The blue segments in the recording indicate the 30 s epochs used for the tonic and phasic current analysis. Right panel: Summary data from 6 recordings where the tonic $GABA_A$R-mediated currents normalized to the capacitance of the cells are plotted before (Control) and during (1 nM DDL-920) the perfusion of the drug. The individual experimental results are illustrated with light gray open circles connected by dotted lines, while the averages (±SEM) are indicated by solid black circles connected by a black dotted line. The p-value indicates a significant reduction of the tonic current as determined using the paired Wilcoxon signed-rank test. (*C*) Plot of the inhibited fraction (efficacy of inhibition; see Materials and Methods for details) of the tonic current vs the same for the phasic current by DDL-920 in cortical PV+INs. The small colored dots are from individual cell recordings while the large dots are the average values with the SD bars extending in both directions. The concentrations of the compounds are color-coded as per the legend. The dashed line has a unity slope and thus indicates no specificity of the compound for either tonic or phasic inhibition [orange data points are from dentate gyrus granule cells (GC) obtained at 1 nM DDL-920]. (*D*) Effects of 100 nM DDL-920 perfused for 15 min on in vitro γ-oscillations in the hippocampal CA3 pyramidal layer. The Morlet wavelets (Bottom panel) show the large enhancement of the magnitude of 40 to 50 Hz oscillations during 1 s epochs before (①) and after (②) the application of DDL-920. (*E*) Comparative effects of 20 min perfusions of 1 or 100 nM DDL-920, or vehicle (aCSF) on the power (RMS averaged during 60 s epochs) of in vitro γ-oscillations (n's represent the number of slices). The changes are expressed relative to the power measured during the baseline recording period (10 min). (*F*) Effects of 5 min perfusions of 100 nM DDL-920 on slices obtained from WT and AD model mice. Measurements as in *E*. The solid lines represent the averages, the dashed lines are the SD envelopes of the averages. There are no significant differences between the enhancement of γ-oscillation power by DDL-920 in the two genotypes.

that it may interfere with GABA binding as part of its NAM mechanism.

Effects of DDL-920 on γ-Oscillations In Vitro. In horizontally cut hippocampal slices we recorded γ-oscillations in an interface-type chamber just below the CA3 pyramidal cell layer in the presence of 50 nM kainic acid (40, 42, 64, 65) (Fig. 2*D*). These oscillations recorded in vitro correspond well to those recorded in vivo during spatial reference memory (64). In this region, the only cells with δ-$GABA_A$Rs are the PV+INs (40). Our previous studies have produced multiple lines of evidence substantiating the expression levels of δ-$GABA_A$Rs on PV+INs effectively controlling γ-oscillation amplitude and frequency recorded in vitro. i) Genetic deletion of δ-subunits and the consequent loss of tonic inhibition onto these INs in $Gabrd^{-/-}$ mice has large potentiating effects on the frequency of in vitro CA3 γ-oscillations (65). More direct evidence came from our studies using conditional knockouts to specifically delete or reduce δ-$GABA_A$R expression *only* in PV+INs (42, 66) resulting in an increased frequency and power of γ-oscillations. Already a 30% reduction in δ-$GABA_A$R in PV+INs significantly increased γ-oscillation frequency (42). Conversely, potentiation of the δ-$GABA_A$R-mediated tonic conductance with neurosteroids lowered the power of γ-oscillations (40). ii) During pregnancy, δ-$GABA_A$R levels on PV+INs decline by about 60% without any change in their PV content. Concomitantly, the frequency of γ-oscillations measured in ex vivo slices from pregnant mice increases considerably (40). In vivo, these altered γ-oscillations are counterbalanced by the increased levels of allopregnanolone during pregnancy to potentiate the function of the reduced number of δ-$GABA_A$Rs on PV+INs just sufficiently to restore the normal (lower) range of γ-oscillations frequency (40).

Based on these findings, our next step was to examine the effects of DDL-920, the NAM of the α1β2δ $GABA_A$Rs of PV+INs, on γ-oscillations recorded in vitro (Fig. 2*D*). The power of the γ-oscillations was evaluated as the RMS of the 30 to 120 Hz band-pass filtered local field potential (LFP). This value was computed for every 60 s of the recordings (Fig. 2 *E* and *F*). We demonstrated similar increases in γ oscillatory power after perfusion of 1 or 100 nM DDL-920 for 20 min (Fig. 2*E*), while perfusion of the artificial cerebro-spinal fluid (ACSF) with no drugs had no effects on the power of γ-oscillations (Fig. 2*E*). We measured the change in power (RMS) divided by average baseline power during each 60 s as in Fig. 2*E* (a value of 1 corresponds to a 100% increase in γ-oscillatory power over that recorded during the baseline). After 15 min of washout, the power of the γ-oscillations was still increased by ~2.5-fold after administration of 1 or 100 nM DDL-920 for 20 min (Fig. 2*E*). The 20 min perfusion duration in the interface chamber will correspond to the shorter perfusion time in the submerged chamber used for studying the DDL-920 effects on tonic inhibition (Fig. 2 *B* and *C*), so that at 1 nM concentration, DDL-920 was effective on both the tonic inhibition and γ-oscillations in vitro. This finding indicates that, at least in vitro, the maximal efficacy of DDL-920 on increasing the power of the γ-oscillations and reached at 1 nM, a concentration that blocks >75% of tonic inhibition of PV+INs with only a negligible effect on their phasic inhibition (Fig. 2*C*).

Once we demonstrated the boosting effects of DDL-920 on γ-oscillations in ex vivo slices of WT mice, we examined its effects on oscillations recorded in slices of AD model mice (see *Materials and Methods* for details). As shown in Fig. 2*F*, we found similar large enhancements in the power (RMS) of γ-oscillations recorded in the hippocampal CA3 pyramidal layer of slices after a 5 min perfusion of 100 nM DDL-920 of WT (n = 6 slices, three mice) and AD model mice (n = 6 slices, three mice), which at this short perfusion time is not expected to reach a steady-state in the interface chamber. Clearly, more studies will be required to establish the proper dose–response effects of DDL-920 in vitro, but our results in AD mice lead us to test the effects of DDL-920 on γ-oscillations in vivo.

Effects of DDL-920 on γ-Oscillations In Vivo. Based on our previously published findings, we had good reason to believe that reducing the effectiveness of tonic inhibition of PV+INs in vivo will boost the power of γ-oscillations. We noticed that the expression levels of δ-$GABA_A$Rs of PV+INs fluctuate during the ovarian cycle and the γ-oscillation frequency and power fluctuate correspondingly (66). For example, during the estrus phase of the cycle, when the δ-$GABA_A$R expression in PV+INs is diminished by about 30%, the amplitude of γ-oscillations is increased by a commensurate amount (66). Notably, similar alterations in γ-oscillations are also found in healthy women during the menstrual cycle (67).

The inverse correlation between δ-$GABA_A$R expression in PV+INs and γ-oscillation power in vivo is promising, but prior to examining the potential effectiveness of DDL-920 on γ-oscillations in vivo, we had to ensure that the drug was permeable through the BBB and that it had a reasonable pharmacokinetic (PK) profile following subcutaneous (SQ) or oral (PO) administration. Mice (n = 3/dose) were given DDL-920 SQ at 1, 5, 10 mg/kg and PO at 10 mg/kg. Plasma and brain were collected 1 and 3 h after drug administration. Targeted liquid LC–MS/MS assay was developed for measurement of DDL-920 concentrations. *SI Appendix*, Fig. S3*A* shows that 1 h after 10 mg/kg DDL-920 SQ injection the maximal concentration (C_{max}) of the drug in the brain reaches about 25 nM, but it declines to ~10 nM after 3 h. The same dose 1 h after oral gavage reaches a C_{max} of ~30 nM but lasts for a longer period (*SI Appendix*, Fig. S3*B*), and after oral pipette administration reaches a C_{max} of ~23 nM. Furthermore our in vitro ADME data show that DDL-920 has good kinetic solubility at >100 μM in water, plasma stability with $t_{1/2}$ > 180 min with a free unbound fraction (F_u) of 34% in brain tissue homogenates (*Materials and Methods* and *SI Appendix,* Table S1), suggesting that the concentration of unbound DDL-920 in the brain is above the in vitro efficacious dose for γ-oscillation enhancement seen in brain slices (Fig. 2*E*). These findings made us confident that a few hours following SQ or oral administration, DDL-920 will reach the brain in sufficient amounts to antagonize tonic inhibition of PV+INs (Fig. 2 *B* and *C*) and thus enhance γ-oscillations.

We first administered DDL-920 (n = 5) or saline (n = 3) to adult WT mice in which bilateral hippocampal electrodes were implanted in the CA1 region to record LFP 24/7 using a chronic tethered recording setup (66, 68). We injected 10 mg/kg SQ during the middle of their light cycle (at around 12 PM) and monitored the hippocampal LFP for several hours prior and after the injection. The 120 s segments used for the analyses were randomly selected from epochs where the RMS of θ-oscillations was from periods of 1 to 3 h before and 2 to 3 h after injections, all chosen from epochs with continuous power (RMS) above baseline in the θ frequency (5 to 12 Hz) filtered recordings. We chose the θ frequency to guide us for the γ-oscillation segments because of the tight phase amplitude coupling (PAC) between the phase of θ-oscillations and γ-oscillation amplitude, a process considered critical for cognition and short-term/working memory (20, 69–71). This approach yielded epochs with similar γ-oscillation powers during the presaline or pre-DDL-920 administration periods (average ± SEM RMS presaline: 13.25 ± 2.47 e-3 mV^2 n = 3 vs. pre-DDL-920: 14.80 ± 1.44 e-3 mV^2 n = 5, P = 0.3929, Wilcoxon signed-rank test). Fig. 3 *A*–*G* illustrates several properties of the γ-oscillations and their PAC to θ-oscillations in an animal that

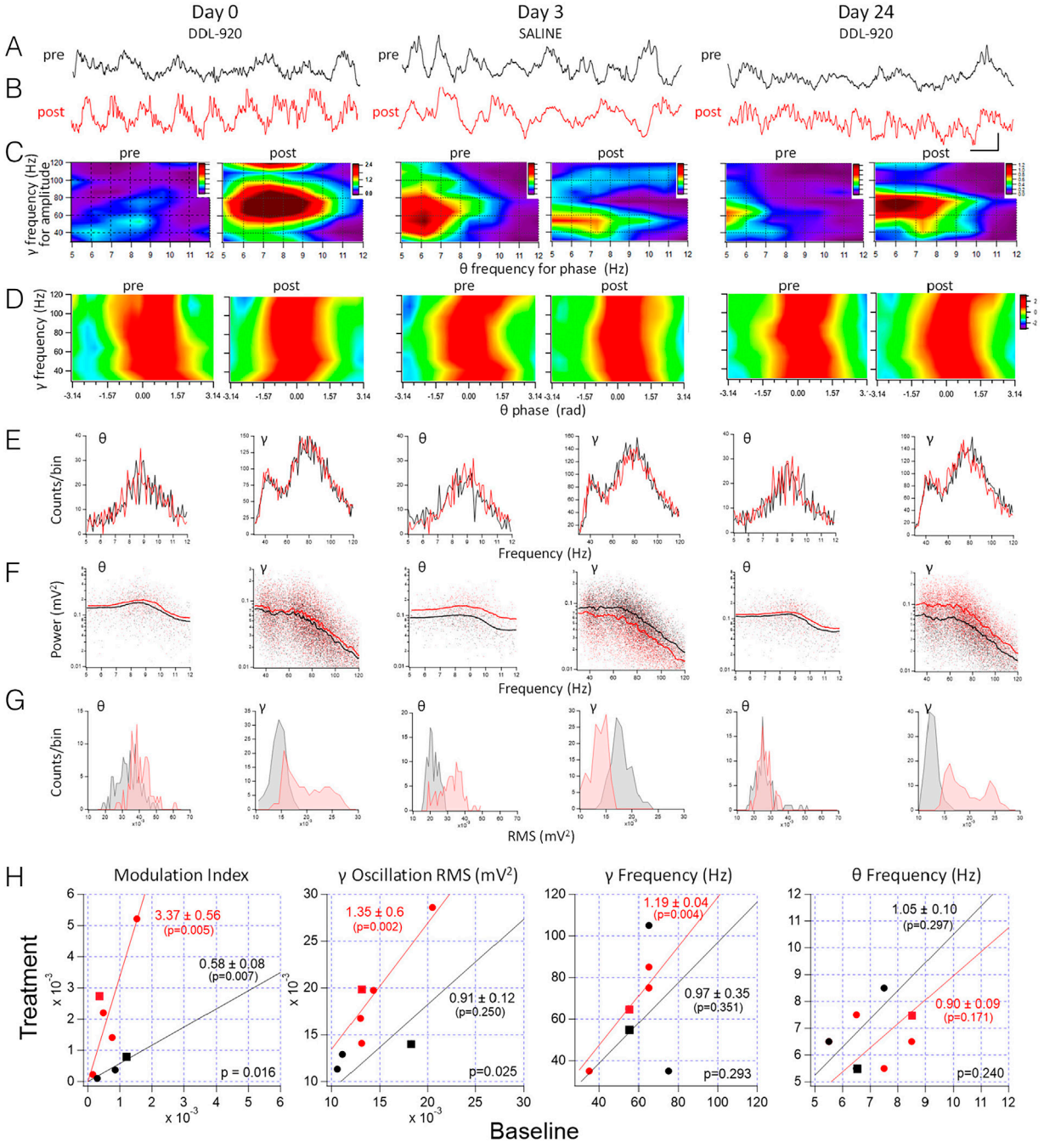

Fig. 3. Effects of DDL-920 (10 mg/kg) SQ in vivo administrations on hippocampal θ- and γ-oscillations in wild type mice. (*A*–*G*) The effects of two DDL-920 injections >3 wk apart in a WT mouse, with an intercalated saline injection 3 d after the first DDL-920 injection. (*A*) The traces are raw recordings of 1 s long epochs taken between 1 and 3 h prior and (*B*) ~3 h, ~2 h, and ~2.5 h, after the DDL-920, saline, and DDL-920 injections, respectively. Calibration bars are 100 ms and 0.2 mV and refer to all traces in *A* and *B*. (*C*–*G*) Analyses of θ–γ frequencies, frequency-amplitude (FAC), and phase- amplitude coupling (PAC) in 120 s segments randomly extracted during the indicated periods before and after the injections. (*C*) MI matrix for θ–γ frequencies during the corresponding 120 s before and after injection epochs. The MI shows by how much γ amplitude for each θ frequency bin deviates from a uniform distribution [Kullback–Leibler distance between two distributions (70, 71)]. Each of the plots is on the same color scale (0 to 1.2 e-3), except for Day 0 post, which is in the scale of 0 to 2.4 e-3. Note the large increases in the MI only after DDL-920 injections. (*D*) PAC of θ–γ oscillations with θ phase represented from trough (−π) to peak (0) and back to trough (+π). The values are z-scores calculated within each 10 Hz frequency bin from 30 to 120 Hz. Despite large increases in γ-oscillation amplitudes, their coupling to θ phase remains unaltered after DDL-920. (*E*) Histograms of the instantaneous frequencies (in Hz) of the θ- and γ-oscillations before (*black*) and after (*red*) injections showing no differences in the frequencies. Note the presence of both low and high γ-oscillation frequencies. (*F*) Instantaneous amplitude vs frequency (in Hz) of θ- and γ-oscillations before (black) and after (red) injections showing increases in the γ-oscillation amplitudes across all frequencies after DDL-920 injections. Please note the log scale of the amplitudes. (*G*) Histograms (at bin widths of 0.001 mV^2) of RMS measured over 120 s of θ- and γ-oscillations before (black) and after (red) DDL-920 injections showing large increases in the γ-oscillation RMS after DDL-920 administrations. (*H*) The parameters indicated on the top of the graphs are plotted as post vs. preinjection values (DDL-920: red n = 5 mice, five injections, only the first injection was included from the mouse shown in panels *A*–*G*; saline: black, n = 3 mice, three injections, including the one from the mouse in panels *A*–*G*. The data points from this mouse are indicated by square symbols). The slopes of the linear regressions through the origin are shown next to the respective regression lines. The *P*-values in the lower right corners of the plots refer to the comparisons between the two slopes. The slopes (±SD) of the MI and of the γ-oscillation RMS are significantly larger after DDL-920 injection than after saline, indicating that SQ injections of 10 mg/kg DDL-920 potentiated these two measures. In contrast, the frequencies of the θ- and γ-oscillations were not altered by the DDL-920 administration. The *P*-values shown in the respective colors under the values of the slopes denote the differences between the individual regression line slopes and a slope = 1, i.e., the "no change" line. The frequencies were plotted as the midpoint from the largest values within 10 Hz bins (γ-oscillations) and 1 Hz bins (θ-oscillations), and therefore, in each plot two sample points overlap in the plots giving the impression that only four data points are present.

received two SQ DDL-920 injections 3 wk apart and a SQ saline injection 3 d after the first DDL-920 administration. Fig. 3*A* shows 1 s long traces to illustrate typical examples of the θ- and γ-oscillations recorded in this mouse during the three preinjection periods while Fig. 3*B* shows similar traces after the DDL-920 or saline injections. The times before and after the injections are indicated in the legend. The modulation index (MI) of the γ-oscillation amplitude by the phase of the θ-oscillations at a given frequency (70, 71) calculated for the entire duration of the 120 s recordings shows a remarkable increase following the two administrations of DDL-920 and no change after saline administration. We also determined the phase of the θ-cycle during which γ-oscillations have the largest amplitude. When measured in 10 Hz bins, the highest amplitude γ-oscillations corresponded with the peak (0 radians on the full scale of $-\pi$ to $+\pi$ radians) of the θ-cycle regardless of θ-oscillation frequency (Fig. 3*D*). This finding is noteworthy, as it means that in spite of the considerable DDL-920-induced increase in the amplitude of γ-oscillations (Fig. 3 *B*, *F*, and *G*), their PAC to θ-oscillations remained constant. We have also plotted the instantaneous frequencies (Fig. 3*E*) and amplitudes (Fig. 3*F*) of the θ- and γ-oscillations recorded during the 120 s representative epochs. The frequency distributions were remarkably unaltered (Fig. 3*E*) showing peaks of 8 to 9 Hz for θ-oscillations and two peaks (~40 and ~80 Hz) for the low and high γ-oscillations, respectively. Accordingly, while DDL-920 increased the power of γ-oscillations, it did not alter their frequencies. Fig. 3*F* shows the log-scaled peak-to-peak amplitudes of the θ- and γ-oscillations plotted against their instantaneous frequencies. The amplitudes of the θ-oscillations increased after each of the three injections, including after saline. In contrast, γ-oscillation amplitudes increased (by 15 to 55%) over their entire frequency range following DDL-920 injections and decreased after saline injection. We also plotted the histograms of the instantaneous power (RMS) of the θ- and γ-oscillations during the same recording periods (Fig. 3*G*). Spectrograms over long time periods (for 4 h before, and for 4 h after the SQ injections) of the γ-oscillations for the same injections (*SI Appendix*, Figs. S5–S7) better illustrate the comparisons between the power of γ-oscillations during the pre- and postinjection times. Summary data from the DDL-920 and saline injections are depicted in Fig. 3*H*. The lines fitted to the data indicate that only the θ-phase γ-amplitude MI (5.8-fold) and the γ-oscillation power (RMS; 1.48-fold) were enhanced by DDL-920 when compared to saline injections, whereas the frequencies of θ- and γ-oscillations were unaffected, as was θ-oscillation RMS. No other parameter was affected by saline injection, except the θ-γ PAC MI which became reduced by 42% (Fig. 3*H*). This could mean that the MI may be exquisitely sensitive to the mild stress induced by the handling and SQ injections in WT animals. Clearly, the DDL-920 effect on the MI must overcome the reduction induced by the handling and injection. Nevertheless, following SQ DDL-920 or saline injections, we did not observe any potential adverse side effects such as hyperexcitability, abnormal spiking, or changes in motor behavior. We have measured the aggregate motor activity patterns derived from the video recordings averaged during 3 h before and 3 h after the DDL-920 or saline injections. The mean ± SD of RMS (in video pixel units) of the motor activities (n = 8 injections, n = 4 mice) prior to DDL-920 administration was 6.85 ± 5.56. This was not significantly different than the value measured after the injection (7.12 ± 2.42; $P = 0.38$, Wilcoxon signed-rank test). Similarly, the pre- and postsaline injection activity levels (n = 6 injections, n = 3 mice) did not differ from each other (pre: 8.02 ± 5.72 vs. post: 8.55 ± 4.49; $P = 1$, Wilcoxon signed-rank test).

Effects of DDL-920 on AD Model Mice Cognitive/Memory Performance. Encouraged by the superior PK of DDL-920 after oral administration (*SI Appendix*, Fig. S3*B* and Table S1) we decided to examine its effects in AD model mice following oral administration with a pipettor. *SI Appendix*, Fig. S8 *A* and *B* show that this route of administration increases γ-oscillation power in AD model mice for about 4.5 h, indicating a coarse measure of its pharmacodynamic effect. We administered DDL-920 by this method to 3 AD mice implanted with bilateral recording electrodes in the CA1 region of the hippocampus. The recordings for the analyses were chosen just as for the WT mice and 1 s long epochs both before and after the DDL-920 (10 mg/kg) administration to one of these mice is shown in Fig. 4*A*. The instantaneous amplitudes of the θ-oscillations were unaffected, but those of γ-oscillations were increased (15 to 35%) over all frequencies, with a significant shift to higher values of the calculated γ/θ amplitude ratios (Fig. 4*B*). In the same mouse, oral saline administration did not produce changes in any of these three parameters (Fig. 4*C*). Similar results were obtained in the other 2 AD mice. Unfortunately, we could not obtain the PAC parameters in these mice, as establishing the location of the electrodes (i.e., ascertain the troughs and peaks of the θ-oscillations) relies on recording sharp wave ripples (68). There were only a few of such events in the AD mice, as they appear to have been replaced by larger amplitude interictal spiking-like activity. The characterization of this phenomenon was beyond the scope of our investigation as similar findings have recently been reported (72).

Next, we wanted to know whether the increase in γ-oscillation power produced by oral administration of DDL-920 in AD mice might be beneficial to ameliorate the cognitive deficits reported in AD mouse models. Our AD model mice were 3-mo-old at the beginning of the experiments ApoE4-TR:5xFAD mice (see *Materials and Methods* for details), as 5xFAD mice of similar age have been shown to be considerably impaired on the memory task in the Barnes maze (73). For 2 wk, and twice a day we treated by oral administration through a pipettor 8 AD mice with vehicle, 7 AD mice with 10 mg/kg DDL-920, and 6 WT mice with vehicle. The treatment schedule and the Barnes maze testing timeline are shown in *SI Appendix*, Fig. S9. By the probe testing day, the animals were 3.75-mo-old. Following treatment, we measured the time spent in the quadrant of the maze containing the escape hole on the 48 h probe day. Fig. 4*D* illustrates that the DDL-920 treated AD mice and the saline-treated WT mice were significantly more likely than the ratio of 0.25 (chance only; statistical tests and p-values are given in the legend) to spend time in the quadrant where the escape hole was previously located. In addition, the vehicle-treated AD mice had significantly longer latencies (Fig. 4*E*) to find the escape hole (mean ± SEM: 34.04 ± 8.68 s; median: 24.35 s; n = 8 mice) than the DDL-920 treated AD mice (10.49 ± 2.41 s; median: 8.9 s; n = 7 mice) or the vehicle-treated WT mice of similar age (6.72 ± 0.96 s; median: 6.65 s; n = 6 mice). The nonparametric Kruskal–Wallis test indicates that at least two of the three groups are significantly different from each other ($P = 0.0002$), and a multiple comparison Tukey test shows that the vehicle-treated AD group is significantly different from the DDL-treated AD group ($P = 0.025$) as well as the vehicle-treated WT group ($P = 0.013$), whereas the DDL-treated AD group is not significantly different from the vehicle-treated WT group ($P = 0.904$; Fig. 4*E*). In the Barnes maze, latency may be regarded as an unreliable measure because it depends on locomotion speed. Therefore, we also compared the path lengths of the animals to the target hole, as this parameter is independent of motor effects

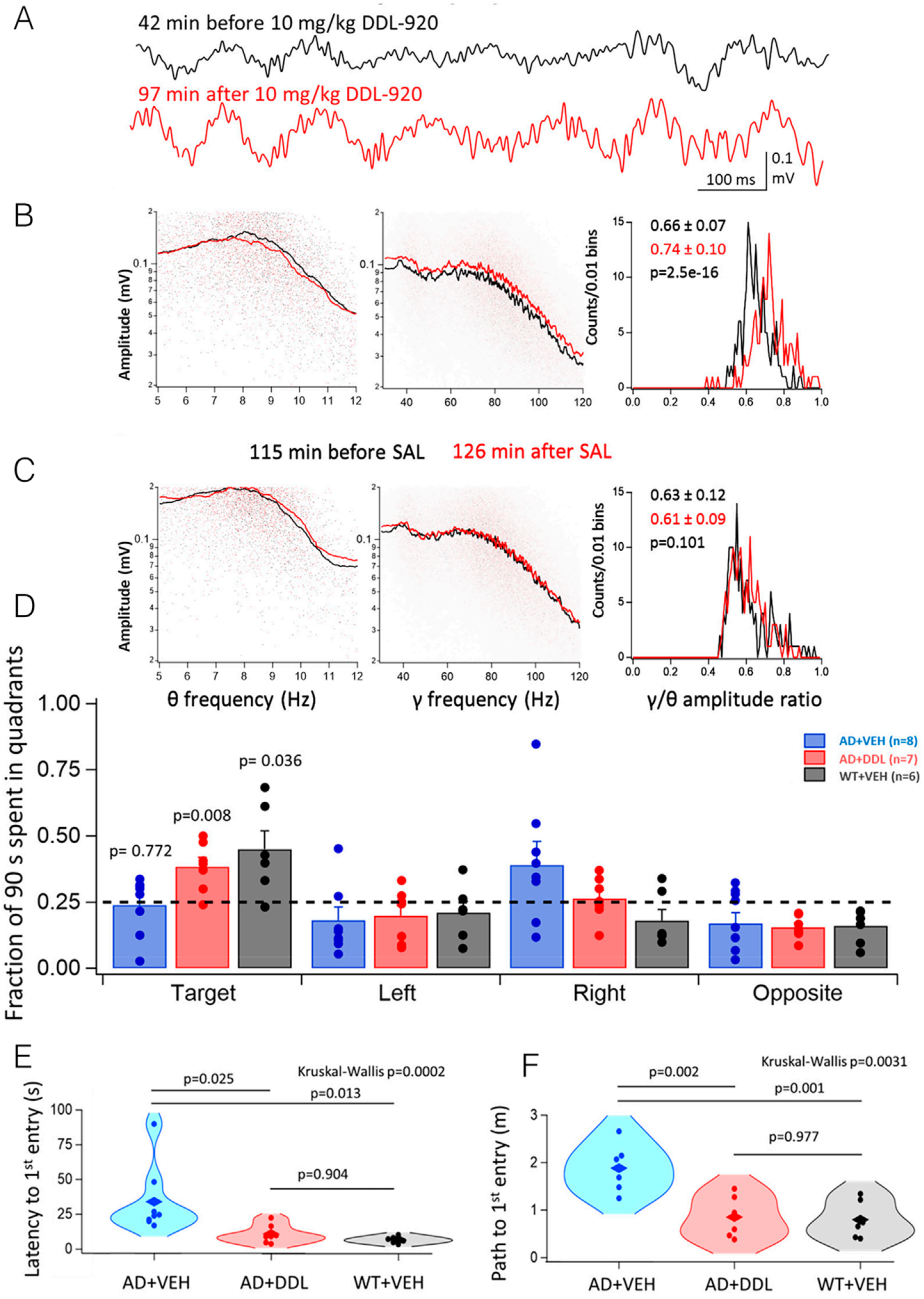

Fig. 4. Effects of DDL-920 (10 mg/kg) oral administration with a pipettor on θ- and γ-oscillations recorded in the hippocampi of AD model mice and on their memory test in the Barnes maze. (*A*) Epochs (1 s long) of in vivo hippocampal recordings of θ and γ-oscillations in an AD model mouse at the indicated times before (black) and after (red) the oral administration of 10 mg/kg DDL-920. (*B*) Instantaneous amplitude vs frequency plots of the θ- (Left panel) and γ-oscillations (Middle panel) in the same mouse obtained from 120 s long epochs at the same times (*black* and *red*) as in *A*. Right panel: Histograms of the 120 measurements over as many s of the ratios of the averaged γ to θ oscillation amplitudes (*P*-values are from *t*-tests). (*C*) Same plots as in *B* for the same mouse after receiving a saline (SAL) oral administration 1 wk after the injection in *A*. Color codes refer to the times before and after SAL administrations. Note the lack of differences between the averaged γ to θ oscillation amplitude ratios after SAL administrations. (*D–F*) After 2 wk of twice-a-day oral DDL-920 (10 mg/kg) or vehicle (VEH) administration, 15 AD mice and 6 WT animals were subjected to a 1-wk training and probe trials in the Barnes maze while still receiving once daily the DDL-920 or SAL oral administration (please see *SI Appendix*, Fig. S9 for details). (*D*) Plot of the fractions of time of the 90 s total time spent in the four quadrants of the Barnes maze (*SI Appendix*, Fig. S9) on probe day 48 h after the last training session. The target quadrant is the quarter area of the maze that previously contained the escape hole. Vehicle (VEH) treated WT mice and DDL-920-treated (DDL) AD mice spent significantly (probabilities indicated on the graph are from a *t*-test comparing the group means to a mean value of 0.25) more time than by chance (0.25) in the target quadrant, whereas the VEH-treated AD mice did no better than chance in this quadrant (*P*-values indicated on the graph are from a *t*-test comparing the group means to a mean value of 0.25). In addition, a nonparametric Kruskal–Wallis test ($P = 0.024$) and a one-way ANOVA ($P = 0.016$) indicate significant differences between the three groups in the target quadrant. Moreover, the multiple comparison Tukey test showed that the WT VEH group was significantly different from the AD VEH group ($P = 0.018$), but not from the AD DDL-920 treated group ($P = 0.642$), which in turn was also significantly different from the AD VEH group ($P = 0.042$). (*E*) Violin plots of the latencies of the first entries to the escape holes on the 48 h probe day after the training has been concluded. Individual data points are shown as solid circles and the mean values are depicted by a rhomboid symbol. The nonparametric Kruskal–Wallis test indicates that at least two groups are significantly different, and the post hoc nonparametric Tukey test comparing all group means shows that the AD+VEH group is significantly different from both other groups, whereas the AD+DDL and WT+VEH group means are not different from each other (*P*-values are indicated on the graph). (*F*) Violin plots of the path lengths until the first entries to the escape holes on the 48 h probe day. Individual data points are shown as solid circles and the mean values are depicted by a rhomboid symbol. The nonparametric Kruskal–Wallis test indicates that at least two groups are significantly different, and the post hoc nonparametric Tukey test comparing all group means shows that the AD+VEH group is significantly different from both other groups, whereas the AD+DDL and WT+VEH group means are not different from each other (*P*-values are indicated on the graph).

(Fig. 4*F*). Vehicle-treated AD mice exhibited significantly longer path lengths (Fig. 4*F*) before finding the escape hole (mean ± SEM: 1.88 ± 0.21 m; median: 1.88 m; n = 8 mice) than the DDL-920 treated AD mice (0.82 ± 0.17 m; median: 0.75 m; n = 7 mice) or the vehicle-treated WT mice of similar age (0.77 ± 0.16 m; median: 0.68 m; n = 6 mice). For the path lengths, the nonparametric Kruskal–Wallis test indicates that at least two groups are significantly ($P = 0.0031$) different from each other, and a multiple comparison Tukey test shows that the vehicle-treated AD group is significantly different from the DDL-treated AD group ($P = 0.002$) as well as the vehicle-treated WT group ($P = 0.001$), whereas the DDL-treated AD group is not significantly different from the vehicle-treated WT group ($P = 0.977$; Fig. 4*F*). We also plotted the total distance run by the mice during the training period and the probe trials and found no differences between the three groups (*SI Appendix*, Fig. S10), indicating long-term DDL-920 treatment caused no side effects affecting motor function while neither weight loss nor adverse events were observed.

Discussion

We describe a unique pharmacological approach meant to enhance cognitive performance and working memory in a state-dependent manner by engaging and amplifying the brain's intrinsic γ-oscillations through enhancing the function of PV+INs. We anatomically and pharmacologically identified $GABA_A$Rs assembled of α1β2δ subunits responsible for the tonic inhibition of PV+INs. We further demonstrated that DDL-920, a small molecule NAM of these receptors, is a potent, efficacious, and selective blocker of the tonic inhibition of PV+INs and consequently enhances γ-oscillations both in vitro and in vivo. Despite the increase in γ-oscillation power, the PAC of θ- and γ-oscillations was not altered by DDL-920, which is important for working memory performance. When administered twice daily for 2 wk, DDL-920 restored the cognitive/memory impairments of 3-mo-old AD model mice as measured by their performance in the Barnes maze. Taken together, our findings indicate that the unique subunit composition of extrasynaptic $GABA_A$Rs of PV+INs should be a valid target for boosting γ-oscillations that could be beneficial in a variety of neurological and psychiatric disorders, including AD.

A remarkable study (25) was the first to describe that optogenetic stimulation of PV+INs or visual stimulation at a characteristic γ-oscillation frequency of 40 Hz reduced the levels of Aβ40/42 in 5XFAD mice, presumably through the involvement of microglial intermediaries. Since the publication of that study, a vast amount of interest has been sparked in adapting the 40 Hz stimulation paradigm to humans (28) for cognitive enhancement therapies, particularly in AD. The noninvasive Gamma ENtrainment Using Sensory stimulation (GENUS) protocol administered daily at 40 Hz for 3 mo has been recently reported to partially benefit early-stage AD patients in a Phase 1 feasibility study (74). In spite of the successful application of various modalities of 40 Hz stimulation to humans, several studies in animals (30–32) have shown that the exogenous 40 Hz stimulation does not entrain endogenous γ-oscillations in the brain, and in some instances, it may actually interfere with the endogenous γ-rhythm. In fact, a recent study (32) found that 40 Hz visual stimulation was effective in reducing the Aβ plaque load in only 1 out of 6 cohorts of AD model mice. In contrast to imposing an exogenous fixed 40 Hz frequency onto the brain, native γ-rhythms of the brain may occur at various frequencies for a given task. Our approach enhances the power of brain-generated γ-oscillations over all its frequencies (30 to 120 Hz) (e.g., Fig. 3*F*). This will ensure that γ-oscillation power will be enhanced regardless of the frequencies demanded by the cognitive or memory tasks engaged by the brain. The mechanism whereby DDL-920 enhances γ-oscillations is probably through increasing the gain of the rhythmic synaptic transmission onto the PV+INs required for these oscillations, both excitatory from principal cells, and inhibitory, from other PV+INs. Tonic inhibition has been identified as a powerful modulator of synaptic gain and function (75), and the synaptic responses of PV+INs are particularly sensitive to changes in the tonic GABA conductance (76). Another possible mechanism to increase γ-oscillation power through regulation of PV+IN function is to increase their firing. Yet, a compound known to increase action potential firing rate in PV+INs by modulating the voltage dependence of Kv3.1/Kv3.2K^+ channels was ineffective in increasing γ-oscillations in slices; however, it did enhance these oscillations once they were dampened by prior administration of Aβ peptides (77). Thus, it is tempting to conclude that selectively reducing the GABA tone in PV+INs may be one of the most effective means of increasing the power of endogenous γ-oscillations in the brain.

An important question remains the applicability of our study to humans. Do PV+INs in the human brain possess the same $GABA_A$R assemblies as we described here for mice? Although there are no direct studies demonstrating this, the α1 subunits are abundant in PV+INs in both macaques (78) and humans. The α1 subunits' close partnership with δ subunits in human PV+INs also awaits direct demonstration, but this dual subunit assembly is highly evident in schizophrenic patients, where α1 and $GABA_A$R δ-subunit mRNA changes are tightly coupled when PV+IN deficits are prevalent (79). Recent human cortex transcriptomics studies also identified the $GABA_A$R δ-subunits with abundant α1 and β2 subunits as distinguishing features of PV+INs (38, 80). There are no specific drugs known to enhance γ-oscillations in humans, but a learned compassion meditation state has been reported to significantly enhance these oscillations (81). It remains to be determined whether trained and frequent practitioners of this type of meditation are less affected by AD.

We are encouraged by the lack of obvious side effects of DDL-920, such as potentially inducing abnormal excitability in the brain, as after all, it is a NAM of inhibitory $GABA_A$Rs. Moreover, we observed no hyperactivity, abnormal behavior, or visible side effects following its long-term (3 wk) administration. More studies will be needed to establish DDL-920's target selectivity, potential toxicity, and off-target effects, but our results so far are promising, and show DDL-920 has good drug-like properties, including stability in human plasma, microsomal stability, and kinetic water solubility. At this time, it is difficult to prove that the enhancement of γ-oscillations in the AD model mice was necessary and sufficient for restoring their cognitive and memory functions. However, the most parsimonious explanation for our findings is that DDL-920 enhanced PV+IN function, that in turn, possibly through enhanced γ-oscillations, led to improved memory and cognition. Our continuing drug development based on DDL-920 as a lead compound will involve additional preclinical testing in other murine models, analysis of AD-related biomarkers, and any off-target effects in the brain along with IND-enabling studies. We are aware of the drawbacks of the applicability of animal models of complex neurodegenerative disorders such as AD to the human condition (82–84). However, at the same time, we are optimistic that a potent and selective orally active small molecule enhancer of γ-oscillations should be beneficial not only in AD especially during its early

stages, but in several neurological and psychiatric disorders including recovery from stroke or posttraumatic brain injury, schizophrenia, depression, ASD, and perhaps also in normal aging-related cognitive deficits.

Materials and Methods

Experimental Model and Study Participant Details. All procedures were performed in accordance with protocols approved by the UCLA Institutional Animal Care and Use Committee (IACUC) and guidelines of the NIH. Mouse strains used were C57BL/6J (Black 6, Jackson Laboratory; JAX stock #000664), JAX stock #003725 (Gabrd$^{-/-}$ mice on a C57BL/6J background), PVcre/Ai14 (JAX stock#017320/#007914). All non-AD mice were 4 to 5 mo old at the time of the experiments. The AD model mice consisted of ApoE-TR mice which express APOE4 under the control of the endogenous mouse APOE promoter were bred to 5xFAD mice (Tg6799) which coexpress five FAD mutations (APP K670N/M671L+I716V+V717I and PS1 M146L+L286V) under the control of the neuron-specific mouse Thy-1 promoter, and backcrossed three times to ApoE-TR mice, resulting in mice homozygous for APOE4, and hemizygous for the 5XFAD transgenes, on a background strain 97% C57Bl/6J and 3% SJL; mice were then inbred between 5xFAD+ and 5xFAD- resulting in littermates E4+/+:FAD+ and E4+/+:FAD−. The AD model mice were 4 to 5 mo old for the in vitro and in vivo electrophysiological recordings, and 3 mo old when training for the Barnes maze experiments were started.

For all other methodological details, including the key resources table, please see *SI Appendix, Materials and Methods*.

Data, Materials, and Software Availability. Numerical data of the figures from manuscript have been deposited in Dryad (https://doi.org/10.5061/dryad.4j0zpc8mw) (85). All new material and mouse models generated from this study will be available upon request. Some may require MTAs.

ACKNOWLEDGMENTS. Parts of this research were supported by National Institutes of Health/National Institute of Aging Grant R01AG050474 andthe Coelho Endowment to I.M., National Institutes of Health/National Institute of Neurological Disorders and Stroke Grant R01NS102608 to C.R.H. We are indebted to Dr. Keith Vossel, Director of the Mary S. Easton Center for Alzheimer's Disease Research and Care who provided funds for research from various anonymous donors to the Center. We thank Professor Greg Cole, University of California Los Angeles Department of Neurology, for providing the initial breeders of the ApoE4-TR:5xFAD mice that were used to generate the cohort for the in vivo studies with DDL-920. We would like to thank W. Sieghart (Medical University of Vienna, Austria) and J.-M. Fritschy (Univ. Zürich, Switzerland) for generously sharing their γ-aminobutyric acid type-A receptor subunit–specific antisera.

Author affiliations: [a]Department of Neurology, The David Geffen School of Medicine at University of California Los Angeles, Los Angeles, CA 90095; [b]Department of Neurosurgery, The David Geffen School of Medicine at University of California Los Angeles, Los Angeles, CA 90095; [c]Department of Neurology, Drug Development Laboratory, Mary S. Easton Center for Alzheimer's Disease Research and Care, The David Geffen School of Medicine at University of California Los Angeles, Los Angeles, CA 90095; [d]Department of Neurobiology, The David Geffen School of Medicine at University of California Los Angeles, Los Angeles, CA 90095; [e]Department of Electrical Engineering, Sapientia Hungarian University of Transylvania, Târgu Mureş 540485, Romania; and [f]Department of Physiology, The David Geffen School of Medicine at University of California Los Angeles, Los Angeles, CA 90095

1. D. Selkoe, E. Mandelkow, D. Holtzman, Deciphering Alzheimer disease. *Cold Spring Harb. Perspect. Med.* **2**, 1–8 (2012).
2. J. Couzin-Frankel, Side effects loom over Alzheimer's drugs. *Science* **381**, 466–467 (2023).
3. N. Swaddiwudhipong *et al.*, Pre-diagnostic cognitive and functional impairment in multiple sporadic neurodegenerative diseases. *Alzheimer's Dement.* **19**, 1752–1763 (2022), 10.1002/alz.12802.
4. V. Ives-Deliperi, J. T. Butler, Mechanisms of cognitive impairment in temporal lobe epilepsy: A systematic review of resting-state functional connectivity studies. *Epilepsy Behav.* **115**, 107686 (2020).
5. I. Litvan *et al.*, Diagnostic criteria for mild cognitive impairment in Parkinson's disease: Movement Disorder Society Task Force guidelines. *Mov. Disord.* **27**, 349–356 (2012).
6. A. K. Godbolt *et al.*, Systematic review of the risk of dementia and chronic cognitive impairment after mild traumatic brain injury: Results of the International Collaboration on Mild Traumatic Brain Injury Prognosis. *Arch. Phys. Med. Rehabil.* **95**, S245–256 (2014).
7. M. C. Lai, M. V. Lombardo, S. Baron-Cohen, Autism. *Lancet* **383**, 896–910 (2014).
8. P. L. Rock, J. P. Roiser, W. J. Riedel, A. D. Blackwell, Cognitive impairment in depression: A systematic review and meta-analysis. *Psychol. Med.* **44**, 2029–2040 (2014).
9. L. Yu *et al.*, Efficacy of transcranial direct current stimulation in ameliorating negative symptoms and cognitive impairments in schizophrenia: A systematic review and meta-analysis. *Schizophr. Res.* **224**, 2–10 (2020).
10. M. Bartos, I. Vida, P. Jonas, Synaptic mechanisms of synchronized gamma oscillations in inhibitory interneuron networks. *Nat. Rev. Neurosci.* **8**, 45–56 (2007).
11. G. Buzsáki, X. J. Wang, Mechanisms of gamma oscillations. *Annu. Rev. Neurosci.* **35**, 203–225 (2012).
12. J. A. Cardin *et al.*, Driving fast-spiking cells induces gamma rhythm and controls sensory responses. *Nature* **459**, 663–667 (2009).
13. G. Chen *et al.*, Distinct inhibitory circuits orchestrate cortical beta and gamma band oscillations. *Neuron* **96**, 1403–1418.e1406 (2017).
14. T. F. Freund, I. Katona, Perisomatic inhibition. *Neuron* **56**, 33–42 (2007).
15. P. Fries, D. Nikolic, W. Singer, The gamma cycle. *Trends Neurosci.* **30**, 309–316 (2007).
16. D. Kim *et al.*, Distinct roles of parvalbumin- and somatostatin-expressing interneurons in working memory. *Neuron* **92**, 902–915 (2016).
17. T. Klausberger, P. Somogyi, Neuronal diversity and temporal dynamics: The unity of hippocampal circuit operations. *Science* **321**, 53–57 (2008).
18. W. Singer, Synchronization of cortical activity and its putative role in information processing and learning. *Annu. Rev. Physiol.* **55**, 349–374 (1993).
19. V. S. Sohal, F. Zhang, O. Yizhar, K. Deisseroth, Parvalbumin neurons and gamma rhythms enhance cortical circuit performance. *Nature* **459**, 698–702 (2009).
20. G. Buzsáki, *Rhythms of the Brain* (Oxford University Press, New York, NY, 2006), p. 464.
21. P. J. Uhlhaas, W. Singer, Neural synchrony in brain disorders: Relevance for cognitive dysfunctions and pathophysiology. *Neuron* **52**, 155–168 (2006).
22. C. J. Stam *et al.*, Generalized synchronization of MEG recordings in Alzheimer's Disease: Evidence for involvement of the gamma band. *J. Clin. Neurophysiol.* **19**, 562–574 (2002).
23. N. Byron, A. Semenova, S. Sakata, Mutual interactions between brain states and Alzheimer's disease pathology: A focus on gamma and slow oscillations. *Biology (Basel)* **10**, 707 (2021).
24. A. Traikapi, N. Konstantinou, Gamma oscillations in Alzheimer's disease and their potential therapeutic role. *Front. Syst. Neurosci.* **15**, 782399 (2021).
25. H. F. Iaccarino *et al.*, Gamma frequency entrainment attenuates amyloid load and modifies microglia. *Nature* **540**, 230–235 (2016).
26. C. Adaikkan *et al.*, Gamma entrainment binds higher-order brain regions and offers neuroprotection. *Neuron* **102**, 929–943.e928 (2019).
27. A. J. Martorell *et al.*, Multi-sensory gamma stimulation ameliorates Alzheimer's-associated pathology and improves cognition. *Cell* **177**, 256–271.e222 (2019).
28. C. Adaikkan, L. H. Tsai, Gamma entrainment: Impact on neurocircuits, glia, and therapeutic opportunities. *Trends Neurosci.* **43**, 24–41 (2020).
29. S. Toniolo, A. Sen, M. Husain, Modulation of brain hyperexcitability: Potential new therapeutic approaches in Alzheimer's disease. *Int. J. Mol. Sci.* **21**, 9318 (2020).
30. K. Duecker, T. P. Gutteling, C. S. Herrmann, O. Jensen, No evidence for entrainment: Endogenous gamma oscillations and rhythmic flicker responses coexist in visual cortex. *J. Neurosci.* **41**, 6684–6698 (2021).
31. T. Lobo, M. J. Brookes, M. Bauer, Can the causal role of brain oscillations be studied through rhythmic brain stimulation? *J. Vis.* **21**, 2 (2021).
32. M. Soula *et al.*, Forty-hertz light stimulation does not entrain native gamma oscillations in Alzheimer's disease model mice. *Nat. Neurosci.* **26**, 570–578 (2023).
33. M. K. van Vugt, A. Schulze-Bonhage, B. Litt, A. Brandt, M. J. Kahana, Hippocampal gamma oscillations increase with memory load. *J. Neurosci.* **30**, 2694–2699 (2010).
34. P. B. Sederberg *et al.*, Hippocampal and neocortical gamma oscillations predict memory formation in humans. *Cereb. Cortex* **17**, 1190–1196 (2007).
35. M. W. Howard *et al.*, Gamma oscillations correlate with working memory load in humans. *Cereb. Cortex* **13**, 1369–1374 (2003).
36. R. Honkanen, S. Rouhinen, S. H. Wang, J. M. Palva, S. Palva, Gamma oscillations underlie the maintenance of feature-specific information and the contents of visual working memory. *Cereb. Cortex* **25**, 3788–3801 (2015).
37. W. Sieghart, M. M. Savic, International Union of Basic and Clinical Pharmacology, CVI: GABAA receptor subtype- and function-selective ligands: Key issues in translation to humans. *Pharmacol. Rev.* **70**, 836–878 (2018).
38. A. Sente *et al.*, Differential assembly diversifies GABA(A) receptor structures and signalling. *Nature* **604**, 190–194 (2022).
39. S. G. Brickley, I. Mody, Extrasynaptic GABA(A) receptors: Their function in the CNS and implications for disease. *Neuron* **73**, 23–34 (2012).
40. I. Ferando, I. Mody, Altered gamma oscillations during pregnancy through loss of delta subunit-containing GABA(A) receptors on parvalbumin interneurons. *Front. Neural Circ.* **7**, 144 (2013).
41. I. Ferando, I. Mody, Interneuronal GABAA receptors inside and outside of synapses. *Curr. Opin. Neurobiol.* **26**, 57–63 (2014).
42. I. Ferando, I. Mody, In vitro gamma oscillations following partial and complete ablation of delta subunit-containing GABAA receptors from parvalbumin interneurons. *Neuropharmacology* **88**, 91–98 (2015).
43. J. Glykys *et al.*, A new naturally occurring GABAA receptor subunit partnership with high sensitivity to ethanol. *Nat. Neurosci.* **10**, 40–48 (2007).
44. I. Milenkovic *et al.*, The parvalbumin-positive interneurons in the mouse dentate gyrus express GABAA receptor subunits alpha1, beta2, and delta along their extrasynaptic cell membrane. *Neuroscience* **254**, 80–96 (2013).
45. S. Olah *et al.*, Regulation of cortical microcircuits by unitary GABA-mediated volume transmission. *Nature* **461**, 1278–1281 (2009).
46. E. Sakalar, T. Klausberger, B. Lasztoczi, Neurogliaform cells dynamically decouple neuronal synchrony between brain areas. *Science* **377**, 324–328 (2022).
47. S. G. Brickley, V. Revilla, S. G. Cull-Candy, W. Wisden, M. Farrant, Adaptive regulation of neuronal excitability by a voltage-independent potassium conductance. *Nature* **409**, 88–92 (2001).

48. P. Kumar *et al.*, Native-state proteomics of Parvalbumin interneurons identifies unique molecular signatures and vulnerabilities to early Alzheimer's pathology. *Nat. Commun.* **15**, 2823 (2024).
49. A. H. Lagrange, N. Hu, R. L. Macdonald, GABA beyond the synapse: Defining the subtype-specific pharmacodynamics of non-synaptic GABAA receptors. *J. Physiol.* **596**, 4475–4495 (2018).
50. K. H. Kaur, R. Baur, E. Sigel, Unanticipated structural and functional properties of delta-subunit-containing GABAA receptors. *J. Biol. Chem.* **284**, 7889–7896 (2009).
51. C. B. Falk-Petersen *et al.*, Discovery of a new class of orthosteric antagonists with nanomolar potency at extrasynaptic GABAA receptors. *Sci. Rep.* **10**, 10078 (2020).
52. V. W. Y. Liao, M. Chebib, P. K. Ahring, Efficient expression of concatenated alpha1beta2delta and alpha1beta3delta GABAA receptors, their pharmacology and stoichiometry. *Br. J. Pharmacol.* **178**, 1556–1573 (2021), 10.1111/bph.15380.
53. N. Zheleznova, A. Sedelnikova, D. S. Weiss, alpha1beta2delta, a silent GABAA receptor: Recruitment by tracazolate and neurosteroids. *Br J. Pharmacol.* **153**, 1062–1071 (2008).
54. N. N. Zheleznova, A. Sedelnikova, D. S. Weiss, Function and modulation of delta-containing GABA(A) receptors. *Psychoneuroendocrinology* **34**, S67–S73 (2009).
55. E. O. Mann, C. A. Radcliffe, O. Paulsen, Hippocampal gamma-frequency oscillations: From interneurones to pyramidal cells, and back. *J. Physiol.* **562**, 55–63 (2005).
56. Y. J. Kang *et al.*, Cell type-specific intrinsic perithreshold oscillations in hippocampal GABAergic interneurons. *Neuroscience* **376**, 80–93 (2018).
57. M. J. Bezaire, I. Raikov, K. Burk, D. Vyas, I. Soltesz, Interneuronal mechanisms of hippocampal theta oscillations in a full-scale model of the rodent CA1 circuit. *eLife* **5**, e18566 (2016).
58. K. A. Wafford *et al.*, Novel compounds selectively enhance delta subunit containing GABA A receptors and increase tonic currents in thalamus. *Neuropharmacology* **56**, 182–189 (2009).
59. M. L. Jensen *et al.*, A study of subunit selectivity, mechanism and site of action of the delta selective compound 2 (DS2) at human recombinant and rodent native GABA(A) receptors. *Br. J. Pharmacol.* **168**, 1118–1132 (2013).
60. V. John, I. Mody, J. J. Campagna, B. Jagodzinska, X. Wei, *Composition and Methods for Treating Neurodegenerative Diseases*, W. I. P. Organization, Ed. (The Regents of the University of California, 2022).
61. P. Wulff *et al.*, Hippocampal theta rhythm and its coupling with gamma oscillations require fast inhibition onto parvalbumin-positive interneurons. *Proc. Natl. Acad. Sci. U.S.A.* **106**, 3561–3566 (2009).
62. M. B. Herd *et al.*, The expression of GABAA beta subunit isoforms in synaptic and extrasynaptic receptor populations of mouse dentate gyrus granule cells. *J. Physiol.* **586**, 989–1004 (2008).
63. S. Zhu *et al.*, Structure of a human synaptic GABA(A) receptor. *Nature* **559**, 67–72 (2018).
64. C. B. Lu, J. G. Jefferys, E. C. Toescu, M. Vreugdenhil, In vitro hippocampal gamma oscillation power as an index of in vivo CA3 gamma oscillation strength and spatial reference memory. *Neurobiol. Learn. Mem.* **95**, 221–230 (2011).
65. E. O. Mann, I. Mody, Control of hippocampal gamma oscillation frequency by tonic inhibition and excitation of interneurons. *Nat. Neurosci.* **13**, 205–212 (2010).
66. A. M. Barth, I. Ferando, I. Mody, Ovarian cycle-linked plasticity of delta-GABAA receptor subunits in hippocampal interneurons affects gamma oscillations in vivo. *Front. Cell. Neurosci.* **8**, 222 (2014).
67. R. L. Sumner *et al.*, Peak visual gamma frequency is modified across the healthy menstrual cycle. *Hum. Brain Mapp.* **39**, 3187–3202 (2018).
68. S. Vrontou *et al.*, Altered brain rhythms and behaviour in the accelerated ovarian failure mouse model of human menopause. *Brain Commun.* **4**, fcac166 (2022).
69. J. E. Lisman, O. Jensen, The theta-gamma neural code. *Neuron* **77**, 1002–1016 (2013).
70. A. B. Tort, R. W. Komorowski, J. R. Manns, N. J. Kopell, H. Eichenbaum, Theta-gamma coupling increases during the learning of item-context associations. *Proc. Natl. Acad. Sci. U.S.A.* **106**, 20942–20947 (2009).
71. A. B. Tort *et al.*, Dynamic cross-frequency couplings of local field potential oscillations in rat striatum and hippocampus during performance of a T-maze task. *Proc. Natl. Acad. Sci. U.S.A.* **105**, 20517–20522 (2008).
72. M. Soula *et al.*, Interictal epileptiform discharges affect memory in an Alzheimer's disease mouse model. *Proc. Natl. Acad. Sci. U.S.A.* **120**, e2302676120 (2023).
73. A. Caccavano *et al.*, Inhibitory parvalbumin basket cell activity is selectively reduced during hippocampal sharp wave ripples in a mouse model of familial Alzheimer's disease. *J. Neurosci.* **40**, 5116–5136 (2020).
74. D. Chan *et al.*, Gamma frequency sensory stimulation in mild probable Alzheimer's dementia patients: Results of feasibility and pilot studies. *PLoS ONE* **17**, e0278412 (2022).
75. A. Semyanov, M. C. Walker, D. M. Kullmann, R. A. Silver, Tonically active GABA A receptors: Modulating gain and maintaining the tone. *Trends Neurosci.* **27**, 262–269 (2004).
76. A. Bryson *et al.*, GABA-mediated tonic inhibition differentially modulates gain in functional subtypes of cortical interneurons. *Proc. Natl. Acad. Sci. U.S.A.* **117**, 3192–3202 (2020).
77. Y. Andrade-Talavera, L. E. Arroyo-Garcia, G. Chen, J. Johansson, A. Fisahn, Modulation of Kv3.1/Kv3.2 promotes gamma oscillations by rescuing Abeta-induced desynchronization of fast-spiking interneuron firing in an AD mouse model in vitro. *J. Physiol.* **598**, 3711–3725 (2020).
78. G. Sperk *et al.*, Immunohistochemical distribution of 10 GABAA receptor subunits in the forebrain of the rhesus monkey *Macaca mulatta*. *J. Comp. Neurol.* **528**, 2551–2568 (2020).
79. J. G. Maldonado-Aviles *et al.*, Altered markers of tonic inhibition in the dorsolateral prefrontal cortex of subjects with schizophrenia. *Am. J. Psychiatry* **166**, 450–459 (2009).
80. B. R. Lee *et al.*, Signature morphoelectric properties of diverse GABAergic interneurons in the human neocortex. *Science* **382**, eadf6484 (2023).
81. A. Lutz, L. L. Greischar, N. B. Rawlings, M. Ricard, R. J. Davidson, Long-term meditators self-induce high-amplitude gamma synchrony during mental practice. *Proc. Natl. Acad. Sci. U.S.A.* **101**, 16369–16373 (2004).
82. K. Mullane, M. Williams, Preclinical models of Alzheimer's disease: Relevance and translational validity. *Curr. Protoc. Pharmacol.* **84**, e57 (2019).
83. M. P. Vitek *et al.*, Translational animal models for Alzheimer's disease: An Alzheimer's Association Business Consortium Think Tank. *Alzheimer's Dement. (N Y)* **6**, e12114 (2020).
84. L. M. Tai, J. Maldonado Weng, M. J. LaDu, S. T. Brady, Relevance of transgenic mouse models for Alzheimer's disease. *Prog. Mol. Biol. Transl. Sci.* **177**, 1–48 (2021).
85. I. Mody, A therapeutic small molecule enhances γ-oscillations and improves cognition/memory in Alzheimer's disease model mice [Dataset]. Dryad. https://doi.org/10.5061/dryad.4j0zpc8mw. Deposited 19 July 2024.